HHS Public Access

Author manuscript

Mater Sci Eng C Mater Biol Appl. Author manuscript; available in PMC 2016 March 07.

Published in final edited form as:

Mater Sci Eng C Mater Biol Appl. 2016 March 1; 60: 357–364. doi:10.1016/j.msec.2015.11.061.

Chitosan-PLGA polymer blends as coatings for hydroxyapatite nanoparticles and their effect on antimicrobial properties, osteoconductivity and regeneration of osseous tissues

Nenad Ignjatović[a], **Victoria Wu**[b], **Zorica Ajduković**[c], **Tatjana Mihajilov-Krstev**[d], **Vuk Uskoković**[b], and **Dragan Uskoković**[a,*]

[a] Institute of Technical Sciences of the Serbian Academy of Science and Arts, Knez Mihailova 35/IV, P.O. Box 377, 11000 Belgrade, Serbia

[b] Advanced Materials and Nanobiotechnology Laboratory, Department of Bioengineering, College of Engineering and College of Medicine, University of Illinois at Chicago, Chicago, USA

[c] University of Niš, Faculty of Medicine, Clinic of Stomatology, Department of Prosthodontics, Bulevar Zorana Djindjica 81, 18000 Niš, Serbia

[d] University of Niš, Faculty of Science and Mathematics, Department of Biology and Ecology, Višegradska 33, P. O. Box 224, 18000 Niš, Serbia

Abstract

Composite biomaterials comprising nanostructured hydroxyapatite (HAp) have an enormous potential for natural bone tissue reparation, filling and augmentation. Chitosan (Ch) as a naturally derived polymer has many physicochemical and biological properties that make it an attractive material for use in bone tissue engineering. On the other hand, poly-D,L-lactide-co-glycolide (PLGA) is a synthetic polymer with a long history of use in sustained drug delivery and tissue engineering. However, while chitosan can disrupt the cell membrane integrity and may induce blood thrombosis, PLGA releases acidic byproducts that may cause tissue inflammation and interfere with the healing process. One of the strategies to improve the biocompatibility of Ch and PLGA is to combine them with compounds that exhibit complementary properties. In this study we present the synthesis and characterization, as well as *in vitro* and *in vivo* analyses of a nanoparticulate form of HAp coated with two different polymeric systems: (a) Ch and (b) a Ch-PLGA polymer blend. Solvent/non-solvent precipitation and freeze-drying were used for synthesis and processing, respectively, whereas thermogravimetry coupled with mass spectrometry was used for phase identification purposes in the coating process. HAp/Ch composite particles exhibited the highest antimicrobial activity against all four microbial strains tested in this work, but after the reconstruction of the bone defect they also caused inflammatory reactions in the newly formed tissue where the defect had lain. Coating HAp with a polymeric blend composed of Ch and PLGA led to a decrease in the reactivity and antimicrobial activity of the composite particles, but also to an increase in the quality of the newly formed bone tissue in the reconstructed defect area.

* Corresponding author at: Institute of Technical Sciences of the Serbian Academy of Science and Arts, Knez Mihailova 35/IV, P.O. Box 377, 11000 Belgrade, Serbia. dragan.uskokovic@itn.sanu.ac.rs (D. Uskoković)..

Keywords

Antimicrobial activity; Bone regeneration; Chitosan; Hydroxyapatite; PLGA; TGA-*on line* MS

1. Introduction

Synthetic nanostructured hydroxyapatite (HAp) over and over again proves to be a material of interest not only for bone tissue engineering, but also for multiple other areas of research, ranging from adsorbents to sensors to optical imaging to controlled drug delivery [1–5]. Enhancement of the properties of HAp proceeds along two main routes: (i) manipulation of microstructure; (ii) combination with other elements and materials. The room for such improvements is apparently limitless. As for the control of microstructure, it is known that parameters such as morphology [6], crystallinity [7], grain [8] and particle size [9,10], topography [11], porosity [12] or compositional gradient [13] have an immense effect on the physical properties and bioactivity of HAp. As for doping HAp, each of its three constitutive ions — calcium, phosphate and hydroxyl — can be substituted with other ions and dozens of chemically different forms of HAp are known so far [14]. Hydrothermal synthesis has been used in our lab to create nanostructured HAp in which calcium ions were substituted with cobalt, and the resulting material exhibited good biological properties during *in vivo* testing [15]. Other ionic substitutions, including predominantly Mg, Zn, Si, Sr, Fe, Co and carbonate, alongside rarer dopants, *e.g.*, K, Na, Se, lanthanides and radionuclides, were noted in the literature [16].

Advancement of nanotechnologies allows for the design of a large number of hybrid, multicomponent systems based on HAp as the central ingredient [17]. Coating HAp particles with bioresorbable synthetic polymers based on poly(lactic-co-glycolic acid) (PLGA) has thus produced materials suitable for filling bone defects [18,19]. Biocompatible polymeric coatings around HAp particles made possible the development of multifunctional nanoparticle systems with immobilized active pharmaceutics, including vitamins and antibiotics [20,21]. Such combinations of soft, polymeric and hard, mineral components are also thought to be the route to creating materials that would mimic the natural properties of bone [22].

Chitosan is a bioderived polysaccharide obtained mainly from shells of crustaceans, corals or jellyfish. Because of its biocompatibility and a range of interesting properties, including antimicrobial, antitumor, anti-inflammatory and immunity-enhancing ones [23–26], chitosan could serve a multifunctional purpose in biomedicine [27]. However, the cationic nature of chitosan can compromise the cell membrane integrity and promote cytotoxicity [28–31]. It can also induce thrombosis [32], and this is what makes the material improper for wider use. There are different strategies for increasing hemocompatibility of chitosan and they are chiefly directed at its chemical modification or mixing with other compounds which exhibit complementary features [33]. HAp particles combined with chitosan, a bioderived polymer, have produced a large interest in bone tissue engineering community because of a generally positive biological response thereto [34,35]. This type of composite material following *in vivo* implantation induced osteon formation, indicating successful vascularization of the

reconstructed defect [36]. Injectable systems based on HAp and chitosan, incorporating bone marrow mesenchymal stem cells, also promoted ectopic bone formation *in vivo* [37]. A three-dimensional (3-D) HAp and chitosan scaffold also proved to be a good substrate for stem cells in regenerative medicine of bone tissue [38]. Also, macroporous 3-D HAp-chitosan scaffolds in form of interconnected networks of polymeric matrices were used to repair damaged or diseased bones [39].

While chitosan can disrupt the cell membrane integrity and is also unsuitable as a blood–contacting biomaterial, the most frequently used synthetic polymer in bone tissue engineering, PLGA, releases acidic byproducts that may cause tissue inflammation and interfere with the healing process [40,41]. One of the strategies to improve the biocompatibility of chitosan and PLGA *per se* may thus be to combine them with compounds that exhibit complementary properties, including one another. The subject of this study is correspondingly nanoparticles of HAp, uncoated and coated with chitosan and chitosan-PLGA polymer blend. Thermogravimetry coupled with mass spectrometry was used for phase identification purposes in the coating process. The obtained powders composed of spherical particles with controlled size distribution were then used as fillers in the reconstruction of artificially formed bone defects *in vivo*. This was preceded by the analysis of their interaction with osteoblastic cells *in vitro* as well as of antibacterial properties against four microbial strains: *S. aureus, S. epidermis, P. aeruginosa, E. coli.* The antimicrobial potency of the synthesized materials was correlated with the osteoregenerative properties evaluated *in vivo*.

2. Materials and methods

2.1. Synthesis of materials

Aqueous calcium nitrate ($Ca(NO_3)_2$) solution (150 ml; 26.6 wt%) was added to the basic solution of ammonium phosphate ($(NH_4)_3PO_4$) (7 ml H_3PO_4 + 165 ml NH_4OH + 228 ml H_2O) at 50 °C and stirred at 100 rpm over the period of 60 min. The solution was then subjected to a heat treatment for 60 min at 100 °C. The obtained gel was then subjected to freeze drying at −10 to −60 °C and under pressures ranging from 0.37 mbar to 0.1 mbar over a period between one and four hours (Christ Alpha 1–2/LD Plus). The obtained product was pure hydroxyapatite powder (HAp) [18].

Chitosan (Ch) of a low molecular weight (Aldrich, deacetylation >75%) dissolved in acetic acid (1 wt%) was mixed with HAp gel in the 4:6 mass ratio while stirring with a magnetic stirrer at 400 rpm. Distilled water was added dropwise to the mixture of chitosan and HAp gel, while stirring at 21,000 rpm (Ultra-Turrax T25, IKA, Germany). The obtained mixture of chitosan and HAp was slowly poured into a glutaraldehyde solution (Grade I, 25% in H_2O) and stirred at the rate of 21,000 rpm for one hour. The resulting mixture was then centrifuged at 5000 rpm and 5 °C for one hour (Hettich Universal 320R). After that, the mixture was decanted, washed twice with distilled water and dried at 20 °C and 1 bar for 12 h in a dry oven (Selecta Vaciotem). The obtained powder was then subjected to freeze drying at −10 to −60 °C, and at pressures ranging from 0.37 mbar to 0.1 mbar for one to six hours. The obtained product was a powder composed of chitosan-coated HAp particles (HAp/Ch) [42].

PLGA (50:50, Sigma, USA) and chitosan, dissolved in acetone and acetic acid, respectively, were mixed with the HAp gel in the mass ratio of 2:2:6. The water solution of poloxamer 188 (polyethylenepolypropylene glycol, 0.1 vol.%) was added dropwise to the mixture of chitosan, PLGA and HAp, while stirring at 21,000 rpm. The obtained mixture of chitosan, PLGA and the HAp was slowly poured into a glutaraldehyde solution (Grade I, 25% in H_2O) and stirred at the rate of 21,000 rpm for one hour. The obtained mixture was then centrifuged at 500 rpm and 5 °C for one hour. After that, the mixture was decanted, washed twice with distilled water and dried at 20 °C and 1 bar for 12 h in a dry oven (Selecta Vaciotem). The obtained powder was then subjected to freeze drying at −10 to −60 °C, and at pressures ranging from 0.37 mbar to 0.1 mbar for one to eight hours. The obtained product was the powder composed of HAp particles coated with chitosan/poly(D,L)-lactide-co-glycolide (HAp/Ch-PLGA) [42].

2.2. Characterization of the materials

X-ray diffraction (XRD) was performed on a Philips PW-1050 diffractometer with Ni-filtered CuKα radiation. Field-emission scanning electron microscopy (FE-SEM) measurements were performed on a MIRA 3 MXU (High resolution SEM, Tescan) microscope. Infrared spectroscopy (FTIR) was done using the KBr technique on a BOMEM MB-100 spectrometer (Hartmann & Braun, Canada) and in the spectral range from 400 to 4000 cm^{-1}. The spectral resolution was 2 cm^{-1}. A simultaneous thermal analysis was performed using Thermo-Gravimetric Analysis/Differential-Thermal Analysis (TGA/DTA), SETSYS 2400 CS Evolution (Setaram Instrumentation) coupled with a gas analysis mass spectrometric system (MS) (Omni Star GSD 320, Pfeiffer). Samples of 10 ± 0.5 mg were analyzed in air atmosphere flow by heating (10 °C/min) them from 28 to 600 °C. The particle size distribution (PSD) was measured on 10 mg/ml of the powder dispersed in water using a Mastersizer 2000 (Malvern Instruments Ltd.) and a *HydroS* dispersion unit for liquid dispersants.

2.3. Antimicrobial activity test (micro-well dilution assay)

in vitro antibacterial activity of HAp, HAp/Ch and HAp/Ch-PLGA was evaluated in reference to laboratory strains of *Escherichia coli* (ATCC 8739), *Pseudomonas aeruginosa* (ATCC 9027), *Staphylococcus aureus* (ATCC 25923), *Staphylococcus epidermidis* (ATCC 12228), and *Candida albicans* (ATCC 10231), using Micro-well Dilution Assay [43]. Prior to the test, the powdered samples were sterilized by means of a UV lamp so as to avoid microorganism impurities. The inocula of the microbial strains were prepared from the overnight broth cultures and suspensions were made in sterile saline (0.9% NaCl). Their optical density was standardized to 0.5 M McFarland solution, corresponding to 10^7–10^8 CFU/mL. Stock solutions of samples were prepared in the sterile potassium hydrogen phosphate buffer. Serial double dilutions were tested in the range of 31.2–0.015 mg/mL, 9.2–0.004 mg/mL and 12.8–0.006 mg/mL in a 96-well microtiter plate with inoculated Mueller-Hinton broth (pH 7.3) for bacteria and Sabouraud dextrose broth (pH 5.6) for yeast (Institute for Immunology and Virology, Torlak, Belgrade). The final volume was 100 μL and the final concentration was 10^6 CFU/mL in each well. The plate was incubated for 24 h at 37 °C. All experiments were performed in triplicates, where two growth controls were included: the corresponding medium with the potassium hydrogen phosphate buffer as a

negative control, and antibiotics tetracycline and nystatin (Appl. Chem) as the positive control. The bacterial growth was determined by adding 20 μL of 0.5% TTC (triphenyl tetrazolium chloride) aqueous solution to the plate. Analysis of variance (ANOVA) was used to determine the statistical significance ($p \leq 0.05$) of the obtained data.

2.4. In vitro experimental design

2.4.1. Cell culture—Mouse calvarial MC3T3-E1 cells were obtained from ATCC and cultured in Dulbecco's modified Eagle medium (DMEM) with 10% fetal bovine serum, 5% antibiotic/antimycotic and 100μg/ml of ascorbic acid to induce differentiation from fibroblastic to osteoblastic lineage.

2.4.2. Immunohistochemistry—MC3T3-E1 cells were plated onto glass coverslips at a density of 5×10^5 cells/well in 24 well plates along with 3 mg of nanopowders. Cells were cultured for 7 days in differentiation media along with nanopowders. At the end of 7 days, cells were washed 1× with PBS to remove excess particles and fixed for 5 min with 4% paraformaldehyde. Cells were then washed 3× in PBS for 5 min each. Fixed cells were incubated for 1 h in 1% bovine serum albumin with 0.1% Triton-X. After blocking, cells were stained with Alexa Fluor 568 Phalloidin (1:400) (*Molecular Probes*) for 1 h at room temperature. After incubation, coverslips were rinsed in 1× PBS and washed for 3 × 5 min in 1× PBS. Cell nuclei were then counterstained using NucBlue fixed cell ReadyProbe reagent (*Molecular Probes*) for 20 min. Images were obtained using a Zeiss LSM 710 confocal microscope (UIC core imaging facility).

2.5. In vivo implantation and histological analysis

Bone regeneration tests were conducted on 20 rats, Wister species. They were divided into two groups: one group, consisting of 5 animals, was the control group, whereas the other one, consisting of 15 animals, was the experimental group. The experimental group was further divided into three subgroups with five animals each. The rats in the first group had HAp powder implanted into the defect; the rats in the second group had HAp/Ch powder implanted into the defect; the rats in the third group had HAp/Ch-PLGA powder implanted into the defect.

The animals from the experimental group had defects introduced on the left side of the mandibular alveolar bone, in the region between the medial line and foramen mentale. The defect was created using a sterile steel borer, 1.6 mm in diameter and 1.8 mm in length depth. The animals had been prepared for this intervention by the application of diazepam (Bensendin, ICN Galenika, Belgrade, Serbia) and were subsequently anesthetized with ketamine hydrochloride USP (Ketalar, Rotexmedica Gmbh, Trittau, Germany). The animals in each group were sacrificed 4 weeks after the implantation. After the mentioned time interval, decalcified samples of the alveolar bone were taken, and after dehydration in a series of alcohol baths, paraffin blocks were made, out of which we took 10 μm wide fragments and counterstained according to the H&E method for histological analysis.

The procedures involving experimental animals were done in accordance with the Guidelines for Work with Experimental Animals adopted by the Ethics Committee of the Faculty of Medicine, University of Niš, Serbia (No 01–2625/2013).

3. Results and discussion

Fig. 1 shows the XRD patterns of HAp, HAp/Ch and HAp/Ch-PLGA. The most intense peaks, observed at 31.8° (2 1 1), 32.2° (1 1 2), 32.9° (3 0 0), 25.9° (0 0 2) and 49.5° (2 1 3), originate from HAp. In accordance with the literature (International Center for Diffraction Data, JCPDS file No. 09–432) and our previous studies [18], the so obtained HAp diffractogram indicates a poorly crystalline, non-stoichiometric form. The diffractogram of HAp/Ch confirms the presence of both HAp and Ch. Namely, in addition to the characteristic peaks of HAp, the two reflections detected at 10.2° and 19.7° both originate from Ch [44]. The XRD pattern of HAp/Ch-PLGA displays no peaks originating from PLGA because this polymer is amorphous, which is in accordance with the XRD studies from our previous works [18–20].

The FE-SEM images of HAp, HAp/Ch and HAp/Ch-PLGA are shown in Fig. 2. The particles of HAp displayed a platelet-like morphology (Fig. 2a). However, after coating HAp with Ch (Fig. 2b), rounder particles were obtained compared to pure HAp. HAp/Ch-PLGA (Fig. 2c) particles had spherical morphologies too. The two-stage emulsification process, consisting of synthesis using a high-energy emulsifier and subsequent processing in the centrifugal field, had an important role in the promotion of spherical composite particle shapes.

For the qualitative confirmation of the content of the synthesized powders, HAp/Ch and HAp/Ch-PLGA were analyzed using FT-IR spectroscopy (Fig. 3). The IR spectrum of HAp/Ch (a) possessed exclusively the absorption bands characteristic for HAp and Ch. The double peak with maxima at 1088 and 1035 cm^{-1} is derived from the vibrations of the phosphate group (PO_4^{3-}) of HAp. The broad band in the 3600–3000 cm^{-1} region is due to the stretching vibration of the hydroxyl group in water. The peaks at 1588 cm^{-1} and 1310 cm^{-1} are amide II and amide III bands of chitosan. The sharp band at 2929 cm^{-1} is assigned to ν(CH) of the polysaccharide chitosan [45].

The analysis of the FT-IR spectra of HAp/Ch and HAp/Ch-PLGA reveals significant differences compared to the spectra of single-component materials [42]. Thus, the Ch-derived band at 1655 cm^{-1} decreased in intensity, while the Ch-derived band at 1588 cm^{-1} increased after the coating of HAp with Ch, indicating the possible interaction between the amide groups of Ch and OH^- groups of HAp (Fig. 1a). Likewise, the stretching ν(C = O) vibration of the carbonyl group of pure PLGA exhibits a bathochromic shift from 1756 to 1736 cm^{-1} (Fig. 1b), which might be due to the hydrogen bonding between C = O groups of PLGA and OH or NH_2 groups of HAp or Ch, respectively.

Fig. 4 shows the simultaneously obtained results from TGA and *on-line* MS gas analysis. The TGA curve of synthesized HAp (Fig. 4a) has two noticeable regions. The first region, up to around 250 °C, is associated with the loss of water physisorbed on the surface of the

particles. In the region between 250 and 600 °C, a moderate loss of lattice water occurs, with a total decrease in mass of about 7% at 600 °C. These results are in line with the results of TG analyses of HAp reported by other authors in the temperature interval up to 600 °C [46].

The TGA curve of HAp/Ch (Fig. 4b) suggests that the detected changes in mass for the most part come from chitosan. The mild loss of mass up to 250 °C is associated with the loss of absorbed water. In the 250–600° C interval, there is a pronounced region of 250–300 °C with a significant drop in mass and the nearby 300–450 °C interval with a milder drop. The significant loss of mass in the temperature interval between 306 and 320 °C (Fig. 4b) is caused by the deacetylation of chitosan and is paralleled by the appearance of CH_3COOH in the gas analysis. The release of H_2O, CO, CO_2 and CH_3COOH in the 280–500 °C temperature interval has also been confirmed in FT-IR analyses by other authors [47]. Namely, the thermal degradation of chitosan polymeric chains in air, starting at ~250 °C, involves the pyrolysis of the polysaccharide structure that proceeds with the dissociation of the glycosidic bonds in the first step and is followed by the further decomposition yielding acetic and butyric acids, alongside a series of smaller fatty acids chains in the C3–C6 range [48,49].

As for PLGA, an abrupt loss of mass occurs in the temperature interval between 260 and 400 °C, while a complete degradation is observed at temperatures higher than 400 °C (100% mass loss). The temperature of pyrolysis of PLGA is recorded as low as 255 °C, while its full degradation was noted to occur at the temperature of 400 °C during TGA carried out by other authors [50]. The TGA curve of HAp/Ch-PLGA, shown in Fig. 4c, is largely defined by the mass loss due to the thermal decomposition of Ch and PLGA. In the temperature interval between 260 °C and 400 °C, the loss of HAp/Ch-PLGA mass, beside Ch, comes from PLGA too and is confirmed by the maximum contents of CO_2, H_2O and CH_3COOH in the corresponding MS gas analysis.

The synthesized HAp had a uniform distribution of particles with a diameter d50 = 70 nm (Fig. 5a). Following coating with the polymers, this value naturally increases. Thus, coating HAp with Ch produced particles of spherical morphology (Fig. 2b) and a diameter d50 = 130 nm.

The obtained particle size distribution for HAp/Ch (Fig. 5b) suggests that there is a minor possibility of agglomerate formation since only 10% of the fraction of particles turn out to be larger than 260 nm (d90 = 260 nm). Coating the particles of HAp with Ch-PLGA polymer blend also leads to the formation of particles with a spherical morphology, for which d50 = 163 nm (Fig. 5c). HAp particles in all the composites retain the same diameter, and the subsequent increase in the diameter is solely the consequence of coating HAp with Ch or Ch-PLGA. Beside d90 = 820 nm, the tendency to form aggregates of HAp/Ch-PLGA particles can also be observed through the occurrence of visible adhesion between single particles.

The minimal inhibitory concentration (MIC) and the minimal microbicidal concentration (MMC) were different for all the three particle types (Table 1). Based on the results given in Table 1, a smaller amount of HAp/Ch particles had a significant effect on the viability of the

initial bacterial inoculum when compared to HAp and HAp/Ch-PLGA. Considering the MIC and MMC values, the antibacterial efficacy of samples increased in the following order: HAp < HAp/Ch-PLGA < HAp/Ch.

The nanoparticles of HAp exhibited a moderate antibacterial activity against both Gram-positive and Gram-negative bacteria. The antimicrobial properties could be a consequence of the formation of various kinds of highly reactive oxygen species (OH^-, H_2O_2, O_2^-, O_2^{2-}) on the surface of the nanoparticles, causing a lethal damage to the bacteria [51]. Beside a series of factors that define the antimicrobial properties of Ch, such as molecular weight (M_w) and the degree of deacetylation (DD), the positive surface charge density is perhaps the most crucial [52]. The main hypothesis of the antimicrobial activity of Ch is thus grounded in the ionic interaction between its positively charged amino groups and the negatively charged bacterial surface, which induces the permeability of the bacterial membrane, though without bacteriophages or Shiga toxins [53]. In our earlier research we determined the zeta potential values for the given particles at pH 6.5, corresponding to the average of the pH of the two broths utilized in this study (Mueller-Hinton – pH 7.3, Sabouraud dextrose – pH 5.6): HAp (−7.9 ± 0.8 mV), HAp/ Ch-PLGA (+3.0 ± 0.3 mV) and HAp/Ch (+18.3 ± 1.9 mV) [42]. Interestingly, as the zeta potential values increase from the negative to the positive, so does the antimicrobial potency of the three different types of particles – HAp, HAp/Ch-PLGA, HAp/Ch, respectively – increase too. Density of the most reactive functional groups in Ch (an amino/ acetamido group at position C-2, secondary and primary hydroxyl groups at positions C-3 and C-6, respectively) [54] is largest on the surface of HAp/Ch, and its highest antimicrobial potency is therefore to be expected.

The results of an immunohistochemistry analysis of the nanoparticle/cell interface demonstrated a relatively viable contact for all the three particles types (Fig. 6). Still, when compared to the perfect integration of pure HAp with the osteoblastic cell population *in vitro*, some level of reservation of the cells in relation to both forms of polymer-coated HAp is evident from the confocal optical micrographs presented in Fig.6. Zones adjacent to the particle surface and wholly vacated by cells are thus occasionally present in micrographs of cells incubated with HAp/Ch and HAp/Ch-PLGA. A possible reason may be the minor presence of glutaraldehyde and polyethylenepolypropylene glycol on the surfaces of HAp/Ch and HAp/Ch-PLGA, respectively, contributing to the mild repulsion experienced by the cells. Still, no adverse morphological indications were observed in the osteoblastic cells, suggesting that all the particle types could be potentially successfully applied for *in vivo* reconstruction of bone defects.

Histological images of osseous defects filled with HAp, HAp/Ch and HAp/Ch-PLGA powders four weeks after the reconstruction are shown in Fig 7. The area of the defect reconstructed with the material with the largest antimicrobial potency (HAp/Ch) exhibited the presence of inflammatory cells, lymphocytes, as well as of some amount of the implanted material (Fig 7c). “Race for the surface” is the term describing the competitive adherence of bacteria and bone cells onto the surface of freshly implanted biomaterials [55]. Its implication is that surfaces attracting the bone cells effectively attract the bacteria too. Conversely, this means that materials that are intensely antimicrobial in nature may be

expected to induce somewhat adverse effects upon implantation in the body, including a more intense inflammation.

Four weeks after the reconstruction with HAp/Ch-PLGA, the bone defect is seen filled with the newly grown bone tissue with Haversian canals present in it (Fig. 7d). High quality of the newly formed tissue is also reflected in the presence of cement lines. The appearance of the Haversian system with blood vessels after only four weeks following the reconstruction of the defect using HAp/Ch-PLGA is a strong indicator of accelerated osteogenesis. Blending Ch with PLGA earlier proved to be valid for the purpose of enhancing the properties of Ch, particularly its cellular uptake [56]. The number of osteoblast cells, as well as their proliferation, also happened to be the largest on the surface of the polymer blend Ch-PLGA, when compared to pure HAp and HAp/Ch [57]. Our research concordantly demonstrates the viability of blending Ch with PLGA in these composite systems.

4. Conclusion

Utilizing the solvent/non-solvent precipitation method, along with freeze-dry processing, hydroxyapatite (HAp) nanoparticles were synthesized and subsequently coated with chitosan (HAp/Ch) and chitosanpoly-D,L-lactide-co-glycolide (HAp/Ch-PLGA) polymer blend. A thermogravimetric analysis coupled to *on-line* mass spectrometry confirmed the coating of the nanoparticulate HAp with Ch and with the Ch-PLGA blend. An immunohistochemistry analysis of the nanoparticle/cell interface demonstrated a relatively viable contact for all the particle types, though with a very minor level of reservation of osteoblastic cells in relation to both forms of polymer-coated HAp particles when compared to pure HAp. HAp/Ch exhibited the highest antimicrobial activity, but after the reconstruction of the bone defect it also caused visible inflammatory reactions in the newly formed tissue where the defect had lain. Blending chitosan coating with PLGA led to a decrease in the reactivity and the antimicrobial activity of the composite particles, but also to an increase in the quality of the newly formed bone tissue in the reconstructed defect area.

Acknowledgements

The research presented here was supported by the Ministry of Education, Science and Technological Development of the Republic of Serbia, under Project No. III45004, and by the United States National Institutes of Health grant R00-DE021416. The authors acknowledge Nenad Petrović of the University of Niš for the assistance in biological experiments, and Maja Kuzmanović, MSc., of the Institute of Technical Sciences of the Serbian Academy of Science and Arts for the assistance with TGA-MS measurements.

References

1. Dorozhkin SV. Nanosized and nanocrystalline calcium orthophosphates. Acta Biomater. 2010; 6:715–734. [PubMed: 19861183]
2. Uskoković V, Uskoković D. Nanosized hydroxyapatite and other calcium phosphates: chemistry of formation and application as drug and gene delivery agents. J. Biomed. Mater. Res. Part B Appl. Biomater. 2011; 96:152–191 B. [PubMed: 21061364]
3. Mahabole MP, Aiyer RC, Ramakrishna CV, Sreedhar B, Khairnar RS. Synthesis, characterization and gas sensing property of hydroxyapatite ceramic. Bull. Mater. Sci. 2005; 28:535–545.
4. Gagnon P, Ng P, Zhen J, Aberin C, He J, Mekosh H, Cummings L, Zaidi S, Richieri R. A ceramic hydroxyapatite-based purification platform. Simultaneous removal of leached Protein A, aggregates, DNA, and endotoxins from MABs. BioProcess Int. 2006; 4:50–60.

5. Altinoglu EI, Adair JH. Near infrared imaging with nanoparticles. Wiley Interdiscip. Rev. Nanomed. Nanobiotechnol. 2010; 2:461–477. [PubMed: 20135691]
6. Uskoković V, Batarni SS, Schweicher J, King A, Desai TA. Effect of calcium phosphate particle shape and size on their antibacterial and osteogenic activity in the delivery of antibiotics in vitro. ACS Appl. Mater. Inter. 2013; 5:2422–2431.
7. Lee WH, Zavgorodniy AV, Loo CY, Rohanizadeh R. Synthesis and characterization of hydroxyapatite with different crystallinity: effects on protein adsorption and release. J. Biomed. Mater. Res. A. 2012; 100:1539–1549. [PubMed: 22419559]
8. Lukić MJ, Jovalekić Č, Marković S, Uskoković D. Enhanced high-temperature electrical response of hydroxyapatite upon grain size refinement. Mater. Res. Bull. 2014; 61:534–538.
9. Dey D, Das M, Balla VK. Effect of hydroxyapatite particle size, morphology and crystallinity on proliferation of colon cancer HCT116 cells. Mater. Sci. Eng. C. 2014; 39:336–339.
10. Sun JS, Tsuang YH, Chang WH, Li J, Liu HC, Lin FH. Effect of hydroxyapatite particle size on myoblasts and fibroblasts. Biomaterials. 1997; 18:683–690. [PubMed: 9152000]
11. Mealy, J.; O'Kelly, K. Cell response to hydroxyapatite surface topography modulated by sintering temperature. J. Biomed. Mater. Res. A. 2015. http://dx.doi.org/10.1002/jbm.a.35487 [Epub ahead of print]
12. Nadra I, Boccaccini AR, Philippidis P, Whelan LC, McGarthy GM, Haskard DO, Landis RC. Effect of particle size on hydroxyapatite crystal-induced tumor necrosis factor alpha secretion by macrophages. Atherosclerosis. 2008; 196:98–105. [PubMed: 17350022]
13. Marković S, Lukić MJ, Škapin SD, Stojanović B, Uskoković D. Designing, fabrication and characterization of nanostructured functionally graded HAp/BCP ceramics. Ceram. Int. 2015; 41:2654–2667.
14. White TJ, ZhiLi D. Structural derivation and crystal chemistry of apatites. Acta Crystallogr. Sect. B: Struct. Sci. 2003; 59:1–16.
15. Ignjatović N, Ajduković Z, Savić V, Najman S, Mihailović D, Vasiljević P, et al. Nanoparticles of cobalt-substituted hydroxyapatite in regeneration of mandibular osteoporotic bones. J. Mater. Sci. Mater. Med. 2013; 24:343–354. [PubMed: 23090835]
16. Uskoković V. Nanostructured platforms for the sustained and local delivery of antibiotics in the treatment of osteomyelitis. Crit. Rev. Their. Drug. 2015; 32:1–59.
17. Venkatesan J, Kim SK. Nano-hydroxyapatite composite biomaterials for bone tissue engineering—a review. J. Biomed. Nanotechnol. 2014; 10:3124–3140. [PubMed: 25992432]
18. Ignjatović NL, Liu CZ, Czernuszka JT, Uskoković DP. Micro- and nano-injectable composite biomaterials containing calcium phosphate coated with poly(DL-lactide-co-glycolide). Acta Biomater. 2007; 3:927–935. [PubMed: 17532275]
19. Ignjatovic NL, Ajdukovic ZR, Savic VP, Uskokovic DP. Size effect of calcium phosphate coated with poly-DL-lactide- co-glycolide on healing processes in bone reconstruction. J. Biomed. Mater. Res. Part B Appl. Biomater. 2010; 94:108–117. [PubMed: 20524184]
20. Ignjatović N, Uskoković V, Ajduković Z, Uskoković D. Multifunctional hydroxyapatite and poly(d,l-lactide-co-glycolide) nanoparticles for the local delivery of cholecalciferol. Mater. Sci. Eng. C. 2013; 33:943–950.
21. Uskoković V, Hoover C, Vukomanović M, Uskoković DP, Desai TA. Osteogenic and antimicrobial nanoparticulate calcium phosphate and poly-(d,l-lactide-co-glycolide) powders for the treatment of osteomyelitis. Mater. Sci. Eng. C. 2013; 33:3362–3373.
22. Uskoković V. When 1 + 1 > 2: nanostructured composites for hard tissue engineering applications. Mater. Sci. Eng. C. 2015; 57:434–451.
23. Smelcerović A, Knezević-Jugović Z, Petronijević Z. Microbial polysaccharides and their derivatives as current and prospective pharmaceuticals. Curr. Pharm. Des. 2008; 14:3168–3195. [PubMed: 19075698]
24. Yin H, Du Y, Zhang J. Low molecular weight and oligomeric chitosans and their bioactivities. Curr. Top. Med. Chem. 2009; 9:1546–1559. [PubMed: 19903163]
25. Arancibia R, Maturana C, Silva D, Tobar N, Tapia C, Salazar JC, Martínez J, Smith PC. Effects of chitosan particles in periodontal pathogens and gingival fibroblasts. J. Dent. Res. 2013; 92:740–745. [PubMed: 23788611]

26. Ing LY, Zin NM, Sarwar A, Katas H. Antifungal activity of chitosan nanoparticles and correlation with their physical properties. Int. J. Biomater. 2012:632698. [PubMed: 22829829]
27. Ravi Kumar MN. A review of chitin and chitosan applications. React. Funct. Polym. 2000; 46:1–27.
28. Loh JW, Yeoh G, Saunders M, Lim LY. Uptake and cytotoxicity of chitosan nanoparticles in human liver cells. Toxicol. Appl. Pharmacol. 2010; 249:148–157. [PubMed: 20831879]
29. Loretz B, Bernkop-Schnurch A. In vitro cytotoxicty testing of non-thiolated and thiolated chitosan nanoparticles for oral gene delivery. Nanotoxicology. 2007; 1:139–148.
30. Qi LF, Xu ZR, Li Y, Jiang X, Han XY. In vitro effects of chitosan nanoparticles on proliferation of human gastric carcinoma cell line MGC803 cells. World J. Gastroenterol. 2005; 11:5136–5141. [PubMed: 16127742]
31. Carreno-Gomez B, Duncan R. Evaluation of the biological properties of soluble chitosan and chitosan microspheres. Int. J. Pharm. 1997; 148:231–240.
32. Balan V, Verestiuc L. Strategies to improve chitosan hemocompatibility: a review. Eur. Polym. J. 2014; 53:171–188.
33. Qiu Y, Zhang N, Kang Q, An Y, Wen X. Fabrication of permeable tubular constructs from chemically modified chitosan with enhanced antithrombogenic property. J. Biomed. Mater. Res. B Appl. Biomater. 2009; 90:668–678. [PubMed: 19213048]
34. Yamaguchi I, Tokuchi K, Fukuzaki H, Koyama Y, Takakuda K, Monma H, Tanaka J. Preparation and microstructure analysis of chitosan/hydroxyapatite nanocomposites. J. Biomed. Mater. Res. 2001; 55:20–27. [PubMed: 11426393]
35. Tavakol S, Nikpour MR, Amani A, Soltani M, Rabiee SM, Rezayat SM, et al. Bone regeneration based on nano-hydroxyapatite and hydroxyapatite/chitosan nanocomposites: an in vitro and in vivo comparative study. J. Nanoparticle Res. 2013; 15:1373–1388.
36. Fernández T, Olave G, Valencia C, Arce S, Quinn J, Thouas G, et al. Effects of calcium phosphate/chitosan composite on bone healing in rats: calcium phosphate induces osteon formation. Tissue Eng. A. 2014; 20:1948–1960.
37. Yu B, Zhang Y, Li X, Wang Q, Ouyang Y, Xia Y, et al. The use of injectable chitosan/nanohydroxyapatite/collagen composites with bone marrow mesenchymal stem cells to promote ectopic bone formation *in vivo*. J. Nanomater. 2013; 2013:8. ID 506593.
38. Ge S, Zhao N, Wang L, Yu M, Liu H, Song A, et al. Bone repair by periodontal ligament stem cell-seeded nanohydroxyapatite-chitosan scaffold. Int. J. Nanomedicine. 2012; 7:5405–5414. [PubMed: 23091383]
39. Zo SM, Singh D, Kumar A, Cho YW, Oh TH, Han SS. Chitosan–hydroxyapatite macroporous matrix for bone tissue engineering. Curr. Sci. 2012; 103:1438–1446.
40. Solheim E, Sudmann B, Bang G, Sudmann E. Biocompatibility and effect on osteogenesis of poly(ortho ester) compared to poly(DL-lactic acid). J. Biomed. Mater. Res. 2000; 49:257–263. [PubMed: 10571914]
41. Tiainen J, Soini Y, Suokas E, Veiranto M, Törmälä P, Waris T, Ashammakhi N. Tissue reactions to bioabsorbable ciprofloxacin-releasing polylactide-polyglycolide 80/20 screws in rabbits' cranial bone. J. Mater. Sci. Mater. Med. 2006; 17:1315–1322. [PubMed: 17143763]
42. Ignjatović N, Vranješ Djurić S, Mitić Ž, Janković D, Uskoković D. Investigating an organ-targeting platform based on hydroxyapatite nanoparticles using a novel in situ method of radioactive 125Iodine labeling. Mater. Sci. Eng. C. 2014; 43:439–446.
43. NCCLS – National Committee for Clinical Laboratory Standards. Performance standards for antimicrobial susceptibility testing: eleventh informational supplement, Document M100-S11. National Committee for Clinical Laboratory Standard; Wayne, PA, USA: 2003.
44. Qi L, Xu Z, Jiang X, Hu C, Zou X. Preparation and antibacterial activity of chitosan nanoparticles. Carbohydr. Res. 2004; 339:2693–2700. [PubMed: 15519328]
45. Kumar R, Prakash KH, Cheang P, Gower L, Khor KA. Chitosan-mediated crystallization and assembly of hydroxyapatite nanoparticles into hybrid nanostructured films. J. R. Soc. Interface. 2008; 5:427–439. [PubMed: 17698476]

46. Kumta PN, Sfeir C, Lee D-H, Olton D, Choi D. Nanostructured calcium phosphates for biomedical applications: novel synthesis and characterization. Acta Biomater. 2005; 1:65–83. [PubMed: 16701781]
47. Corazzari I, Nistico R, Turci F, Faga MG, Franzoso F, Tabasso S, et al. Advanced physico-chemical characterization of chitosan by means of TGA coupled on-line with FTIR and GCMS: thermal degradation and water adsorption capacity. Polym. Degrad. Stab. 2015; 112:1–9.
48. Lopez FA, Merce ALR, Alguacil FJ, Lopez-Delgado A. A kinetic study on the thermal behaviour of chitosan. J. Therm. Anal. Calorim. 2008; 91:633–639.
49. Georgieva V, Zvezdova D, Vlaev L. Non-isothermal kinetics of thermal degradation of chitosan. Chem. Cent. J. 2012; 6:81. [PubMed: 22857524]
50. D'Avila Carvalho Erbetta C. Synthesis and characterization of poly(d,l-lactide-coglycolide) copolymer. J. Biomater. Nanobiotechnol. 2012; 3:208–225.
51. Ragab HS, Ibrahim FA, Abdallah F, Al-Ghamdi AA, El-Tantawy F, Radwan N, Yakuphanoglu F. Synthesis and in vitro antibacterial properties of hydroxyapatite nanoparticles. IOSR J. Pharm. Biol. Sci. 2014; 9:77–85.
52. Kong M, Chen XG, Xing K, Park HJ. Antimicrobial properties of chitosan and mode of action: a state of the art review. Int. J. Food Microbiol. 2010; 144:51–63. [PubMed: 20951455]
53. Jeon SJ, Oh M, Yeo W, Galvão KN, Jeong KC. Underlying mechanism of antimicrobial activity of chitosan microparticles and implications for the treatment of infectious diseases. PLoS ONE. 2014; 9:e92723. [PubMed: 24658463]
54. Kumirska J, Weinhold MX, Thöming J, Stepnowski P. Biomedical activity of chitin/ chitosan based materials—influence of physicochemical properties apart from molecular weight and degree of *n*-acetylation. Polymers. 2011; 3:1875–1901.
55. Gristina AG, Naylor P, Myrvik Q. Infections from biomaterials and implants: a race for the surface. Med. Prog. Technol. 1989; 14:205–224. [PubMed: 2978593]
56. Zeng P, Xu Y, Zeng C, Ren H, Peng M. Chitosan-modified poly(d,l-lactide-co-glycolide) nanospheres for plasmid DNA delivery and HBV gene-silencing. Int. J. Pharm. 2011; 415:259–266. [PubMed: 21645597]
57. Tanir TE, Hasirci V, Hasirci N. Preparation and characterization of chitosan and PLGA-based scaffolds for tissue engineering applications. Polym. Compos. 2015; 36:1917–1930.

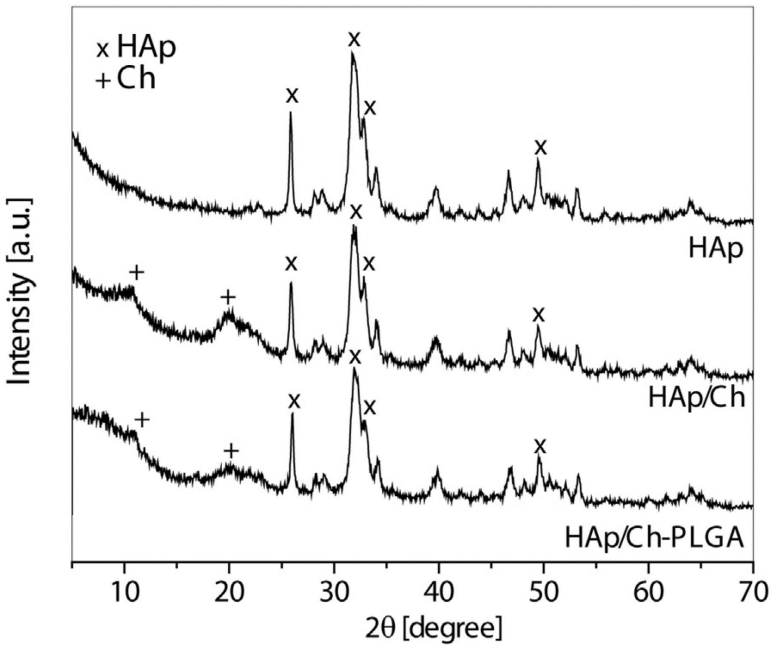

Fig. 1.
XRD of HAp, HAp/Ch and HAp/Ch-PLGA.

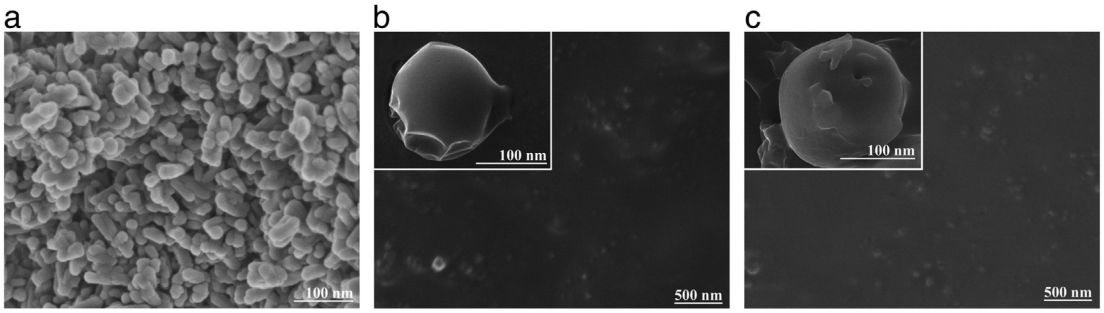

Fig. 2.
FE-SEM of HAp (a), HAp/Ch (b) and HAp/Ch-PLGA (c).

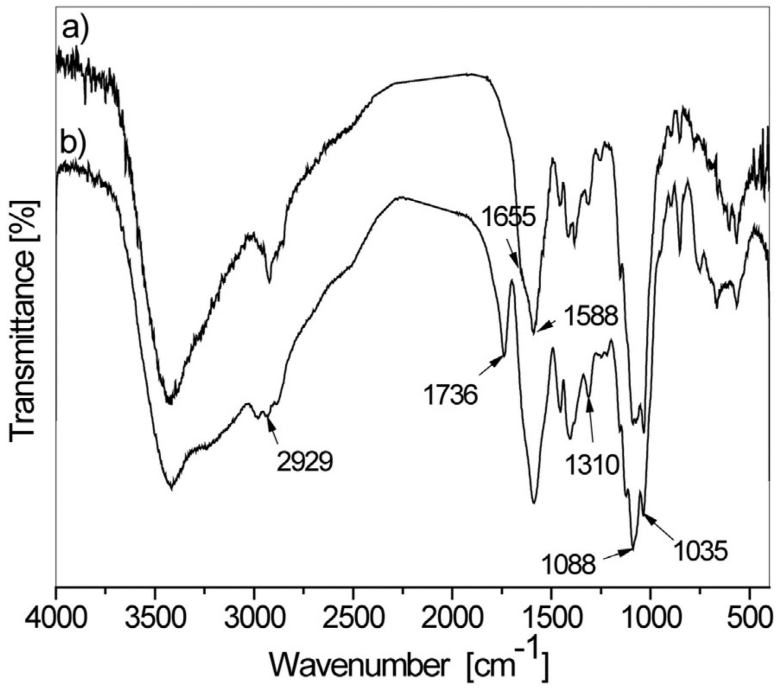

Fig. 3.
FT-IR spectra of HAp/Ch (a) and HAp/Ch-PLGA (b).

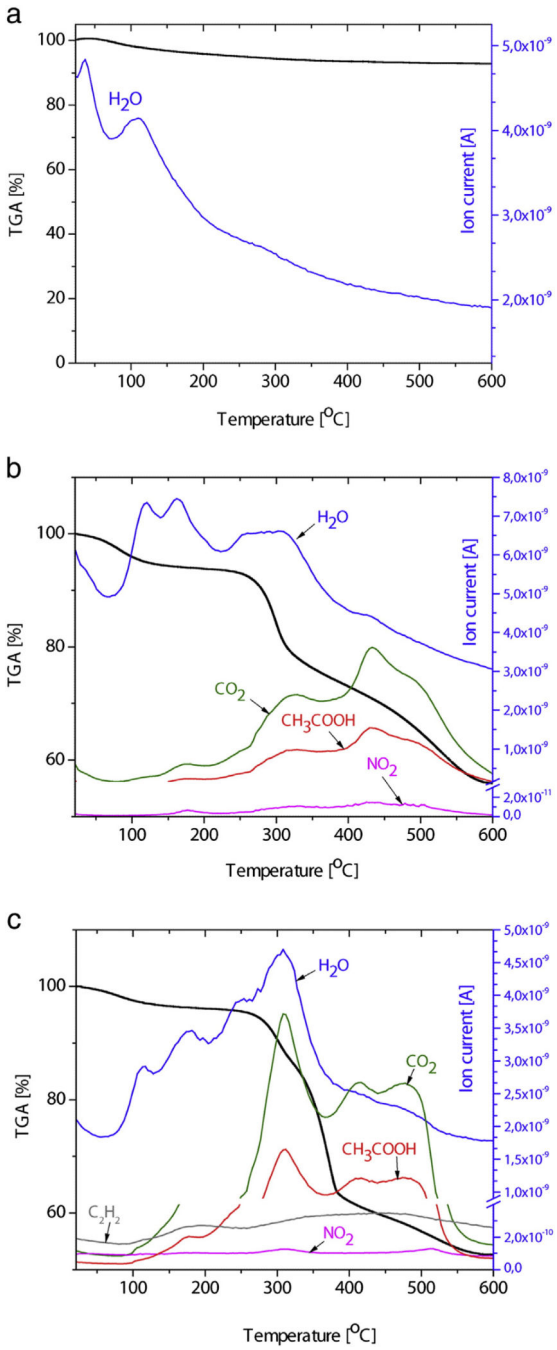

Fig. 4.

Thermal Analysis: TGA-*on line* MS (gas analysis) of HAp (a), HAp/Ch (b) and HAp/Ch-PLGA (c).

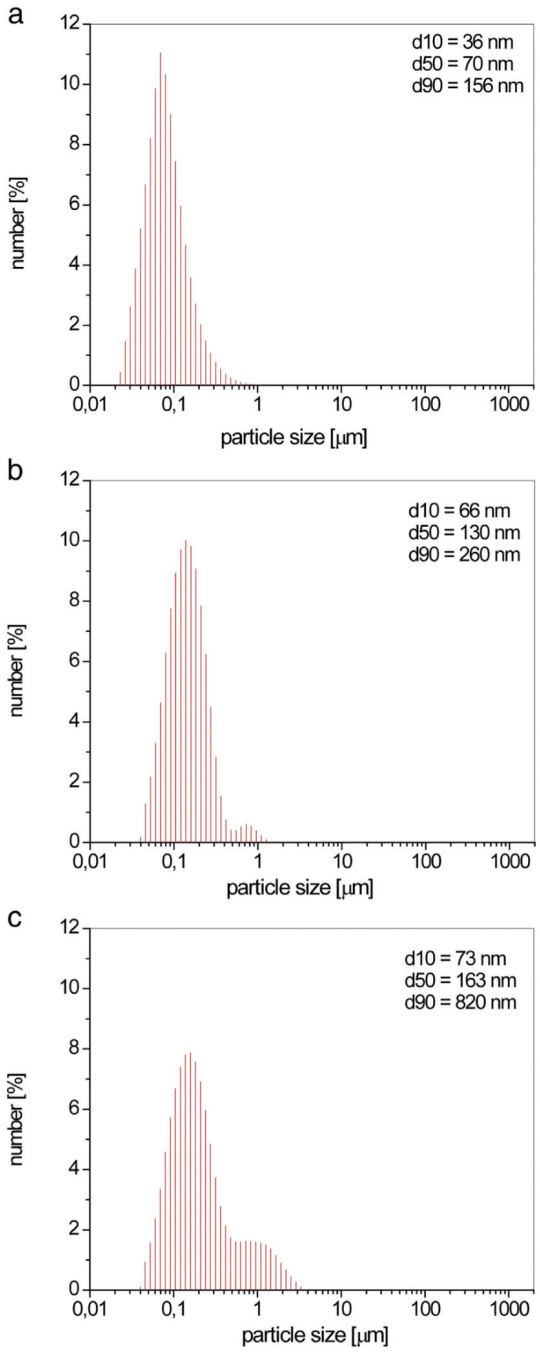

Fig. 5.
Particle size distribution of HAp (a), HAp/Ch (b) and HAp/Ch-PLGA (c).

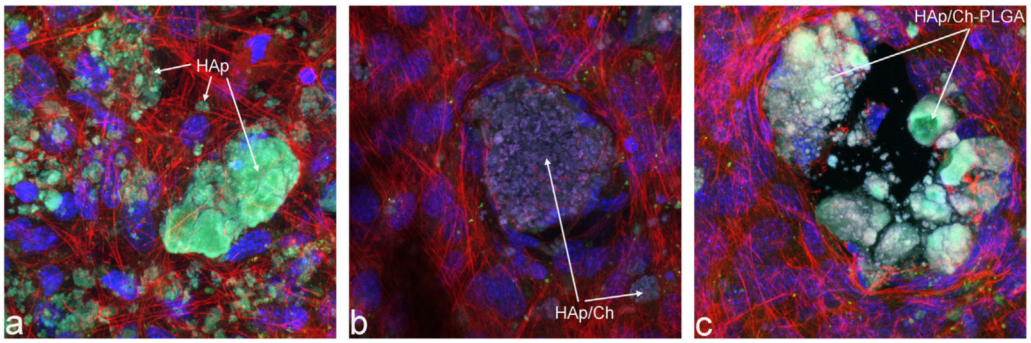

Fig. 6.

Confocal optical micrographs of fluorescently stained osteoblastic MC3T3-E1 cells following incubation with HAp (a), HAp/Ch (b) and HAp/Ch-PLGA (c). Cell nuclei are stained in blue and f-actin microfilaments are stained in red. (For interpretation of the references to colour in this figure legend, the reader is referred to the web version of this article.)

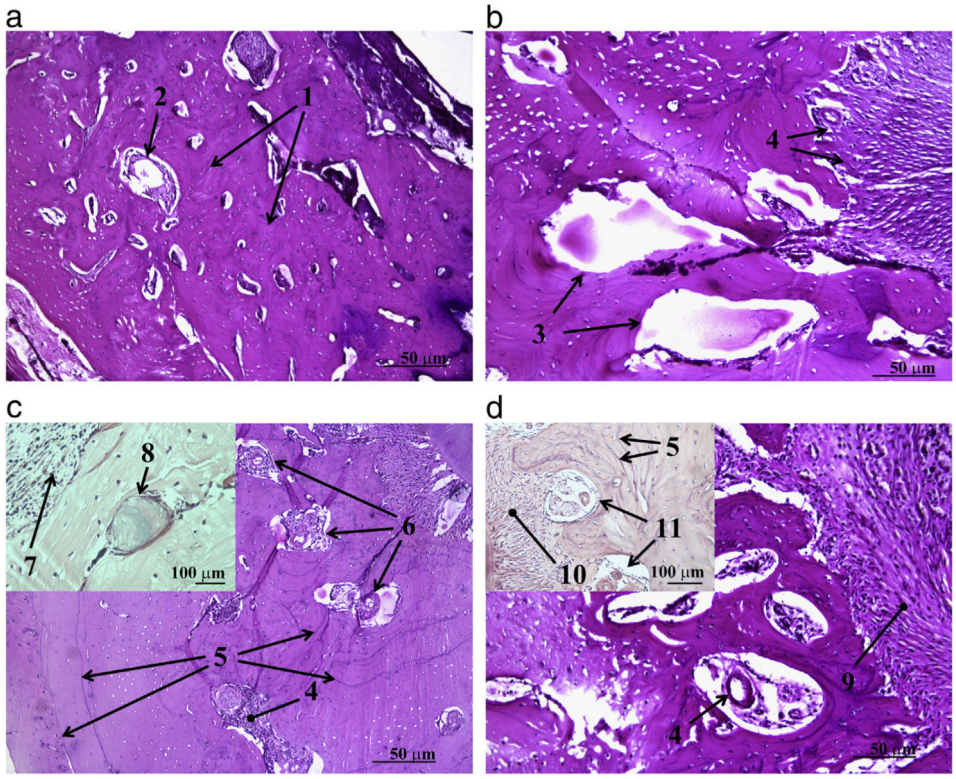

Fig. 7.

Histological analysis of the control and experimental groups of animals four weeks after the implantation: control (a), HAp (b), HAp/Ch (c) and HAp/Ch-PLGA (d). [1 — new bone tissue; 2 — blood vessel; 3 — filling defect with new tissue; 4 — implant material in substitution phase; 5 — cement lines; 6 — fibroblasts + fibrocytes; 7 — inflammatory cells — lymphocytes; 8 — implant material in substitution phase, surrounded by bone tissue and osteoblasts; 9 — osteogenesis; 10 — periosteum; 11 — Haversian canals with blood vessels and nerves].

Table 1

The antimicrobial activity of HAp, HAp/Ch, HAp/Ch-PLGA and of referent antibiotics (MIC/MMC in mg/mL).

Microbial strains	Source	HAp		HAp/Ch		HAp/Ch-PLGA		Antibiotic *	
		MIC (mg/mL)	MMC (mg/mL)	MIC (mg/mL)	MMC (mg/mL)	MIC (mg/mL)	MMC (mg/mL)	MIC (mg/mL)	MMC (mg/mL)
Escherichia Coli [–g]	ATCC 8739	31.20	31.20	9.20	>9.20	12.80	12.80	0.001	0.001
Pseudomonas aeruginosa[–g]	ATCC 9027	15.60	31.20	4.60	9.20	6.40	12.80	0.004	0.032
Staphylococcus aureus [+g]	ATCC 25923	15.60	15.60	4.60	4.60	6.40	6.40	0.0005	0.002
Staphylococcus epidermidis[–g]	ATCC 12228	7.80	15.60	2.30	4.60	3.20	6.40	0.0005	0.0005
Candida albicans[f]	ATCC 10231	31.20	31.20	9.20	>9.20	12.80	12.80	0.001	0.002

* Tetracycline for bacteria and Nystatin for fungs; significance ($p \leq 0.05$); Gram-positive bacterium [+g], Gram-negative bacterium [–g], fungs [f].